Max-Planck-Institut
für Mathematik
in den Naturwissenschaften
Leipzig

Modeling and simulation of martensitic phase transitions with a triple point

by

Patrick W. Dondl and Johannes Zimmer

Preprint no.: 95 2003

Modeling and simulation of martensitic phase transitions with a triple point

Patrick W. Dondl*, Johannes Zimmer†

* Division of Engineering and Applied Science,
California Institute of Technology, Pasadena CA 91125, USA
† Max Planck Institute for Mathematics in the Sciences,
Inselstr. 22, 04 103 Leipzig, Germany

Abstract

A framework for modeling complicated global energy landscapes in a piecewise manner is presented. Specifically, a class of strain-dependent energy functions is derived for the triple point of Zirconia (ZrO_2), where tetragonal, orthorhombic (orthoI) and monoclinic phases are stable. After presenting a simple two-dimensional framework to deal with this symmetry breaking, an explicit energy is fitted to the available elastic moduli of Zirconia in this two-dimensional setting. First, we use the orbit space method to deal with symmetry constraints in an easy way. Second, we introduce a modular (piecewise) approach to reproduce or model elastic moduli, energy barriers and other characteristics independently of each other in a sequence of local steps. This allows for more general results than the classical Landau theory (understood in the sense that the energy is a polynomial of invariant polynomials), since the class of functions considered here is strictly larger. Finite Element simulations with the energy constructed here investigate the pattern formation in Zirconia at the triple point.

1 Introduction

This paper provides a framework for modeling complex energetic landscapes, such as atomistic potentials or energies describing materials that undergo phase transitions. Until recently, typically only few physical parameters (such as elastic moduli) were known in these cases, and a simple polynomial interpolation scheme was sufficient to fit this data. *Ab initio* calculations and improved experimental techniques provide a much larger wealth of data which can typically not be fitted easily by a polynomial approach. We present a simple framework to model these energetic landscapes, including symmetry constraints and a possibly large number of parameters to fit. In particular, the framework presented here allows for fitting important physical quantities like energy barriers, which can be difficult to be resolved correctly with a polynomial approach.

To be specific, we have chosen to demonstrate the modeling framework with Zirconia (ZrO_2) as a highly nontrivial example. From the point of view of modeling, one of the specific difficulties of Zirconia (as well as any other material undergoing phase transformations) is its complicated energy landscape, which is invariant under the high symmetry point group in the space of symmetric strains. We provide a theoretical framework by proposing an (isothermal) phenomenological energy density for the tetragonal-orthorhombic (orthoI)-monoclinic (t-o-m) triple point of Zirconia using piecewise functions. Numerical simulations demonstrate the feasibility of this approach. In particular, the flexibility of such a triple point material is compared to that of a two phase solid. Modeling and simulation of martensitic transformations, i.e., diffusion-less first-order solid-solid transformations, is known to be demanding even for two-phase materials (Luskin, 1996; Swart and Holmes, 1992; Reid and Gooding, 1997). We are not aware of comparable simulations of a triple point material.

Fadda et al. (2002) use the ansatz of lowest order invariant polynomials to obtain an energy function and fit most of the elastic moduli. They show that it is impossible to fit all elastic moduli of the tetragonal and the monoclinic phase accurately within this framework. Two elastic moduli of the monoclinic phase, C^m_{25} and C^m_{35}, are too high by an order of magnitude respectively by about 150% with respect to the closest available experimental and theoretical data (elastic moduli for the orthorhombic phase were not considered; no experimental data seems to be available here).

This is another manifestation of the fact that lowest-order polynomials are often not suitable to describe the energetic landscape correctly. Gooding et al. (1991) pointed out that the minimal set of order parameters may lead to unrealistically high estimates for the thermal activation energy. To determine the energy barrier correctly, they use non-symmetry-breaking order parameters or, more specifically, invariant polynomials of higher order. This approach is often difficult and results in steeply growing energy functions. We introduce a related, but novel approach to define elastic energies in terms of piecewise functions. Within the framework of piecewise defined functions, fitting elastic moduli and other parameters reduces to solving local problems and interpolating appropriately.

As demonstrated below for Zirconia, accurate fitting of the energy to given values for the elastic moduli of the different phases (tetragonal, monoclinic and orthorhombic) becomes in this framework a simple task. Since the derived phenomenological energy will serve as input of the two-dimensional simulations in Section 4, we limit ourselves to a suitable plane describing the tetragonal-orthorhombic-monoclinic phase transition and can therefore only fit the moduli visible in this plane. In particular, the moduli that cannot be fitted accurately with the lowest order polynomial ansatz are invisible. We point out, however, that the methods presented in Section 3 are also applicable in the three-dimensional context. Also, the framework presented here is, due to its locality, general enough to accommodate data obtained from *ab initio* calculations, for example energy barriers. Since in this case the representation of the energy will only be substantially longer, we have chosen Zirconia as a suitable

material for explaining the ideas, even if data from *ab initio* calculations for Zirconia is not available.

Besides being advantageous when physical data needs to be fitted, the method of deriving energy functions described here might also be of interest from a theoretical point of view. The Landau-Ericksen theory (Landau, 1967; Ericksen, 1980) commonly used was originally designed for a *local* analysis. There, the aim is to catch the structure of the energy in the vicinity of the bifurcation points only. Polynomials have proven to be an appropriate choice. However, we aim here at reconstructing the *global* energy picture. In this case, there is no justification to rely on polynomials alone. Rather, the ideas presented here seem to be a natural extension of the original ideas of Landau. By gluing together piecewise polynomials, which describe the local picture of the energy landscape appropriately, one gains a global picture. From that point of view, the idea of defining the energy as a piecewise function seems to be quite natural.

We point out that a purely polynomial approach may result in additional stable phases, as reported by Fadda et al. (2002) for an additional orthorhombic phase for Zirconia in a certain temperature regime. It is well possible that an additional phase is just an artefact stemming from the rigidity of polynomials, and will disappear in the piecewise framework described here. Since we focus on the isothermal situation around the triple point, we will not pursue this question here. However, the methods presented in Section 3 will facilitate such an investigation.

The flexibility gained with this piecewise approach comes at a price, however. First, the there is a drop in smoothness from polynomials to the energy function derived here, which will only be C^1. In principle, however, one could use Hermite splines of arbitrary order to obtain an arbitrarily smooth energy. For the simulations, a continuously differentiable function will suffice (see for example Balk et al. (2001); Huo and Müller (2003) for engineering and physics literature with piecewise defined C^0 or C^1 energy densities). In our numerical study of boundary value problems, no spurious effect stemming from the discontinuity in the elastic moduli were ever observed. Second, the energy does not have a representation as compact as a polynomial one, since the class of functions considered here comprises the polynomials. However, one could express it in a reasonably compact way by using base functions (e.g., splines). Since we have no use for this here, we will refrain from doing so and consider the energy just as input of the Finite Element simulation. For such simulations, the complexity of the energy becomes largely irrelevant; the simulations in Section 4 will show that the energy derived here is well suited for scientific computations. Third, the method comes with a huge number of parameters. We minimize the arbitrariness of choosing parameters by fitting the elastic moduli of the different variants and interpolating by solving the biharmonic equation. In that way, essentially only the parameters in the biharmonic equation determine the interpolation (e.g., energy barriers), while suitable variations of other parameters such as the domain of the interpolation do not change the qualitative behavior of the energy landscape.

We remark that these ideas not only apply to multiphase crystals, but also

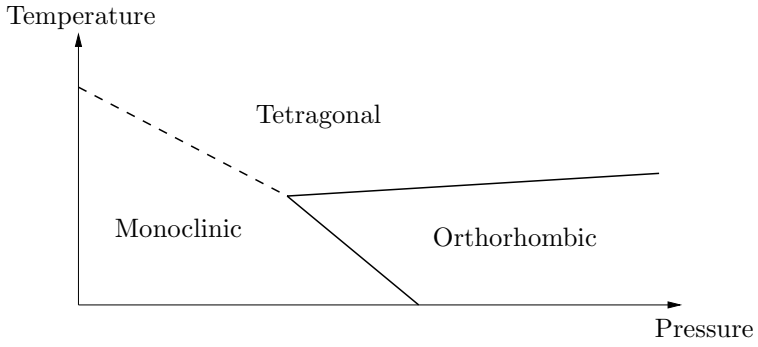

Figure 1: Schematic phase diagram (see Fadda et al. (2002); Ondik and McMurdie (1998). The triple point is near 1.8 GPa and 840°K.

carry over to much more complicated situations, for example energetic landscapes arising in molecular dynamics. Applications of the ideas presented here in that context will be an area of future research. Zirconia has been chosen as a prototype of a material with a triple point due to its relevance for applications. Extraordinary mechanical properties like high corrosion resistance and a melting point at high temperature make Zirconia a potentially very attractive material in engineering ceramics. Zirconia exhibits several solid-solid phase transitions which are responsible for the internal formation of microstructures. The phase changes are also the source of transformation toughening, which is considered to be a milestone in achieving high strength ceramics of high toughness. Zirconia is the most important toughening agent for ceramics. The high pressure and temperature at the triple point (see Figure 1), however, render experimental investigations of the phase transformations difficult. Theoretical modeling and numerical simulations as presented here can provide valuable insight.

Zirconia also proves to be particular challenging for the orbit space methods described in Section 3 since the scaling of the orthorhombic phases as being closer to the tetragonal phase than the monoclinic ones has to be resolved correctly.

The numerical simulations investigate the pattern formation and nucleation in Zirconia. Precisely, we study a dynamic theory of phase transformations in a two-dimensional elastic solid, where the phenomenological energy for Zirconia developed before is used. The main purpose of the simulations is to show that with the piecewise energy defined in Section 3, the three phases of Zirconia can be recovered correctly in a numerical setup, while a lowest-order polynomial energy fails to exhibit clearly distinguishable phases. This is due to the different heights of the energy barriers obtainable with these approach (Figure 3 and the simulations in 4.4). A side theme of the simulation is to demonstrate the flexibility of a three-phase material, as opposed to a two-phase material. It is shown that the size of the boundary layer with high potential energy is significantly smaller for a three-phase material, which indicates a higher flexibility of such a

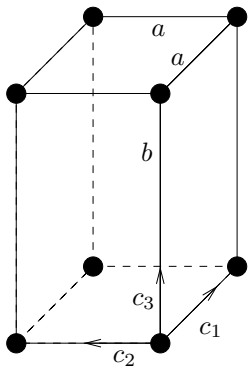

Figure 2: Tetragonal reference configuration. The axes c_1, c_2 and c_3 of rotations in the tetragonal point group are shown.

material (regarding the accommodation of boundary conditions). This suggests that the set of recoverable strains might be larger for a three-phase material than for a comparable two-phase material.

The article is organized as follows. In Section 2, it is shown that the phase transition can be analyzed in a two-dimensional framework. In Section 3, an energy function is derived and fitted to the elastic moduli of the different phases. Numerical simulations using this energy are presented in Section 4. We close with a discussion in Section 5.

2 Planar phase transformation

We follow Truskinovsky and Zanzotto (2002) in considering a transformation path in Zirconia joining the tetragonal phase and certain orthorhombic and monoclinic phases. We show that these phase transformations can be described as an in-plane transformation, which justifies the two-dimensional simulations in Section 4.

As usual, we take the high symmetry phase as reference configuration. (This is justified by the observation that one can define a so-called Ericksen-Pitteri neighborhood (Ericksen, 1980; Pitteri, 1984) of the lattice with the maximal symmetry in such a way that it comprises the lattices with a subgroup symmetry.) For Zirconia, the tetragonal phase, denoted T_3, is the high symmetry phase. To fix the notation, we list the elements of T_3 (Truskinovsky and Zanzotto (2002); the axes c_1, c_2, c_3 are shown in Figure 2; R_a^α stands for the rotation with angle α and axis a):

$$T_3 = \left\{1, R^\pi_{c_1}, R^\pi_{c_2}, R^\pi_{c_3}, R^\pi_{c_1+c_2}, R^\pi_{c_1-c_2}, R^{\frac{\pi}{2}}_{c_3}, R^{\frac{3\pi}{2}}_{c_3}\right\}.$$

The orthorhombic subgroups of T_3 are

$$O_{1,2,3} := \left\{1, R^\pi_{c_1}, R^\pi_{c_2}, R^\pi_{c_3}\right\}$$

and

$$O_{3,1\pm2} := \left\{1, R^\pi_{c_3}, R^\pi_{c_1+c_2}, R^\pi_{c_1-c_2}\right\},$$

see Truskinovsky and Zanzotto (2002). Both orthorhombic groups form their own conjugacy class in T_3.

There are three conjugacy classes of monoclinic subgroups, from which we list one representative each:

$$M_{1,2} := \left\{1, R^\pi_{c_1}\right\}, \qquad M_{1\pm2} := \left\{1, R^\pi_{c_1+c_2}\right\}, \qquad M_3 := \left\{1, R^\pi_{c_3}\right\}.$$

Of course, there is also the trivial triclinic subgroup {Id}. A schematic representation of the point groups is given by Truskinovsky and Zanzotto (2002, Figure 3).

We assume the symmetry breaking in ZrO_2 occurs along the path

$$T_3 \longrightarrow O_{123} \longrightarrow M_3.$$

This transformation path different from the one usually considered for the tetragonal-monoclinic transformation responsible for the transformation toughening (Fabris et al., 2000). It is the path suggested by Truskinovsky and Zanzotto (2002); Fadda et al. (2002) based on experimental evidence collected there.

We study this phase transformation using a continuum theory by invoking the Cauchy-Born rule (Ericksen in Gurtin, 1984). Let $\Omega \subset \mathbb{R}^3$ be the reference configuration. The deformation of the crystal is given by $y(x)$. The displacement is defined as $u(x) := y(x) - x$. The deformation gradient is

$$F_{ij} := \frac{\partial y_j}{\partial x_i}.$$

According to the Cauchy-Born rule, this deformation gradient serves as a measure of the deformation of the lattice.

It is well known that there are several variants of the low-symmetry phases, where the number of variants is given by the quotient of the order of the high symmetry group and the order of the low symmetry group (see, e.g., Bhattacharya, 2003, Section 4.3).

For the reader's convenience, the deformation gradients for the different variants are listed below; see Truskinovsky and Zanzotto (2002). In particular, it can be seen that the symmetry breaking takes place in the c_1c_2-plane shown in Figure 2, to which we therefore restrict ourselves. Consequently, the third row and column of the deformation gradients are always given by $(0, 0, 1 + u_{33})$ and will be suppressed from notation. For O_{123}, there are two variants,

$$F = \begin{pmatrix} 1+u_{11} & \\ & 1+u_{22} \end{pmatrix} \text{ and } F = \begin{pmatrix} 1+u_{22} & \\ & 1+u_{11} \end{pmatrix}.$$

Similarly, for M_3, there are four variants. It is easy to see that the corresponding deformation gradients F are given by the four matrices

$$\begin{pmatrix} 1+u_{11} & \pm u_{12} \\ \pm u_{12} & 1+u_{22} \end{pmatrix} \text{ and } \begin{pmatrix} 1+u_{11} & \pm u_{12} \\ \pm u_{12} & 1+u_{22} \end{pmatrix}.$$

Finally, deformation gradients preserving the tetragonal symmetry are of the form

$$F = \begin{pmatrix} 1+u_{11} & \\ & 1+u_{11} \end{pmatrix}.$$

In the c_1c_2-plane depicted in Figure 2, the tetragonal phase T_3 is characterized by a C_4 symmetry (the symmetry of a square). This group is generated by a counterclockwise rotation by 90°, which will be denoted by σ. The two orthorhombic phases have a planar C_2 symmetry, since their restriction to the c_1c_2-plane is a rectangle. Finally, monoclinic variants reduce in the c_1c_2-plane to parallelograms, which also have C_2 as the planar point group. But for monoclinic phases, three-dimensional rotations by 180 degrees along any axis in the c_1c_2-plane are no longer a self-mapping. Restricted to the c_1c_2-plane, this means that for monoclinic phases, reflections are no longer self-mappings.

3 Derivation of an phenomenological free energy density

The main input to the Finite Element simulation will be a phenomenological energy function modeling the relevant physical properties of Zirconia. Fadda et al. (2002); Truskinovsky and Zanzotto (2002) have shown that, for the traditional approach based on invariant polynomials of lowest order, it is not possible to fit all available elastic moduli of Zirconia exactly. We will use the orbit space approach, where these problems are avoided and local geometrical considerations allow for a comparatively simple construction. We refer the reader to Zimmer (2003a) for a detailed presentation of the orbit space method. Here, it suffices to know that 'orbit space' is a quotient, which can intuitively be seen as a map identifying all variants of the same phase, while separating unrelated variants. We introduce two new ideas to fit elastic moduli and control the growth of the energy at the energy barriers and infinity. The first idea is to define the energy as a piecewise function. This turns the problem of fitting elastic moduli and other data into finding the solutions of several local problems which need to be interpolated appropriately. The second idea is to interpolate between the minima by solving the biharmonic equation with a Finite Element code. Again, locality makes it easy to adjust the energy barriers between the minima to a desired height. The biharmonic equation has been chosen for its resemblance to the variational principle of minimal curvature. In this way, only few parameters need to be controlled. Also, the Finite Element simulation of the biharmonic equation automatically returns splines.

The axiom of frame indifference and the polar decomposition imply that the energy function can be written as a function of $E := \frac{1}{2}\left(F^TF - \mathrm{Id}\right) \in \mathrm{Sym}(2,\mathbb{R})$. Here, E is the Green-St. Venant strain tensor, and $\mathrm{Sym}(2,\mathbb{R})$ is the space of symmetric real matrices, which will from here on be identified with $\mathbb{R}^3$. Point

groups act on this set by conjugation,

$$\begin{aligned} P \times \mathrm{Sym}(2,\mathbb{R}) &\to \mathrm{Sym}(2,\mathbb{R}) \\ (P,E) &\mapsto PEP^{-1}. \end{aligned}$$

The Green-St. Venant tensor E will be written in the Voigt notation, i.e.,

$$E = \begin{pmatrix} e_1 & \frac{1}{2}e_6 \\ \frac{1}{2}e_6 & e_2 \end{pmatrix}$$

with $e_i \in \mathbb{R}$. A short calculation shows that the representation of σ on $\mathbb{R}^3 = (e_1, e_2, e_6)$ is given by

$$\tilde{\sigma} = \begin{pmatrix} 0 & 1 & 0 \\ 1 & 0 & 0 \\ 0 & 0 & -1 \end{pmatrix}.$$

Since $\tilde{\sigma}^2 = \mathrm{Id}$, it is immediate that the action of the point group on E is isomorphic to C_2. The orthorhombic and monoclinic subgroups coincide on this space and act both as identity.

The next step is to find invariant polynomials in e_1, e_2 and e_6 under the action of the high symmetry point group. It is a classic theorem due to Hilbert that for compact Lie groups, the algebra of invariant polynomials (that is, multiplication of invariant polynomials is defined) is finitely generated. See, for example, Theorem 2.1.3 in Sturmfels (1993), or Weyl (1997) as the classical reference. An invariant basis can easily be computed automatically, for example with Singular (Greuel et al., 2001). Here it is even possible to guess a basis:

$$\begin{aligned} \rho_1(e_1,e_2,e_6) &:= e_1 + e_2 \quad \text{(the trace of } E\text{)}, \\ \rho_2(e_1,e_2,e_6) &:= e_1^2 + e_2^2 \quad \text{(the radius squared)}, \\ \rho_3(e_1,e_2,e_6) &:= e_6^2. \end{aligned} \tag{1}$$

It is immediate that none of these invariants can be expressed as a combination of the two remaining invariants. Therefore, they are independent. We need to show that they form a basis. According to Chevalley (1955, Theorem (A)), there is a basis of 3 invariants. Since the polynomials listed above are of the lowest possible degree, they form such a basis.

The fact that these three polynomials form a basis of the algebra of polynomials invariant under C_2 means that every such polynomial $\tilde{\rho} = \tilde{\rho}(e_1, e_2, e_6)$ can be written as $\tilde{\rho} = P(\rho_1, \rho_2, \rho_3)$, where P is a polynomial. Such polynomial bases have been given by Smith and Rivlin (1958) for the different crystal classes, where polynomial energy functions were considered. We proceed by demonstrating how to use these bases to define more general multiphase energy functions modeling given mechanical properties (such as location of minimizers and elastic moduli). To do so, we introduce the *Hilbert map* ρ, which is defined as

$$\rho\colon \begin{cases} \mathbb{R}^3 \to \mathbb{R}^3 \\ (e_1,e_2,e_6) \mapsto (\rho_1(e_1,e_2,e_6), \rho_2(e_1,e_2,e_6), \rho_3(e_1,e_2,e_6)). \end{cases}$$

Table 1: Locations of the minima. The minima in the $e_1e_2e_6$-space are calculated from the data given by Fadda et al. (2002, Appendix). We used $p = 1.8155$ GPa and $T = 838.9^{\circ}$K. The values in the orbit space follow by evaluating the Hilbert map $\rho = (\rho_1, \rho_2, \rho_3)$ at these points.

	tetragonal	orthorhombic	monoclinic
e_1	0	0.01	0.0479
e_2	0	0	0.0055
e_6	0	0	0.1600
$\rho_1(e_1, e_2, e_6)$	0	0.01	0.0534
$\rho_2(e_1, e_2, e_6)$	0	0.0001	0.00232
$\rho_3(e_1, e_2, e_6)$	0	0	0.0256

The image of $\mathbb{R}^3$ under the Hilbert map is the *orbit space*. See Zimmer (2003a) for an explanation and more background.

Next, we locate the position of the different phases of Zirconia in the orbit space $\rho(\mathrm{Sym}(2, \mathbb{R}))$. Consider, for example, the orthorhombic phase. In Table 1, the data of one orthorhombic variant is given as $e_1 = 0.01, e_2 = 0, e_6 = 0$. By applying the tetragonal generator σ to this element, we find the other variant as $e_1 = 0, e_2 = 0.01, e_6 = 0$. Both variants are mapped to the same point in the orbit space, namely $(0.01, 0.0001, 0)$. This is a general property of orbit spaces, see, e.g., Zimmer (2003a). Table 1 lists the location of the other minima.

We turn towards the construction of a function Φ on the orbit space such that $\Phi(\rho)$ is a phenomenological energy function modeling the relevant mechanical properties of Zirconia at the *t-o-m* triple point. Since the Hilbert map identifies exactly the symmetry-related variants as one point in the orbit space, Φ can be an arbitrary function. It will be chosen to be a piecewise function. In this way, all available experimental and theoretical data of the elastic moduli can be fitted accurately. The values for the elastic moduli and the locations of the minima are taken from Fadda et al. (2002). No experimental data was available for the orthorhombic phase, so orthorhombic data of a similar magnitude as at the other phases was chosen before fitting the energy function. See Table 2 for the elastic moduli.

The definition of Φ is done in two steps. First, a mesh on the orbit space is created. The *breaks* are the locations where different pieces of the function will be joined. They form *boxes* in a natural way. The breaks are listed in Table 3. A comparison with the location of the minima on the orbit space in Table 1 shows that every minimum is in the interior of one box. On those three boxes, Φ is defined as Φ_t, Φ_o and Φ_m, respectively. These functions are listed in Table 4; they are fitted in a straightforward manner to the elastic moduli given in Table 2.

Second, Φ is extrapolated appropriately, here by a Finite Element approach. We solve the biharmonic equation on the Finite Element space spanned by

Table 2: Elastic Moduli (in GPa). The values for the tetragonal and monoclinic phases are up to rounding errors in the parameters the same as in Fadda et al. (2002, Tables II(b), IV(b)) (orthorhombic data seems to be unavailable). Note also the re-labeling of the indices in the monoclinic phase in Table IV in Fadda et al. (2002). Here, the tetragonal phase's labeling is always used.

	tetragonal	orthorhombic	monoclinic
C_{11}	340	300	312
C_{22}	340	350	350
C_{66}	95.0	90.0	66.3
C_{12}	33.0	33.0	35.2
C_{16}	0	0	3.2
C_{26}	0	0	4.3

Table 3: Location of the breaks for the mesh on the orbit space.

ρ_1	ρ_1 cont.	ρ_2	ρ_2 cont.	ρ_3	ρ_3 cont.
-0.05	0.0125	-0.0005	0.000225	-0.05	0.03
-0.035	0.03	-0.000045	0.001	-0.0015	0.045
-0.02	0.05	-0.00002	0.002	-0.001	0.06
-0.0025	0.056	-0.000005	0.0026	-0.0005	
0.0025	0.07	0.000025	0.004	0.0001	
0.005	0.085	0.00005	0.0055	0.0125	
0.0075	0.1	0.000075	0.007	0.02	

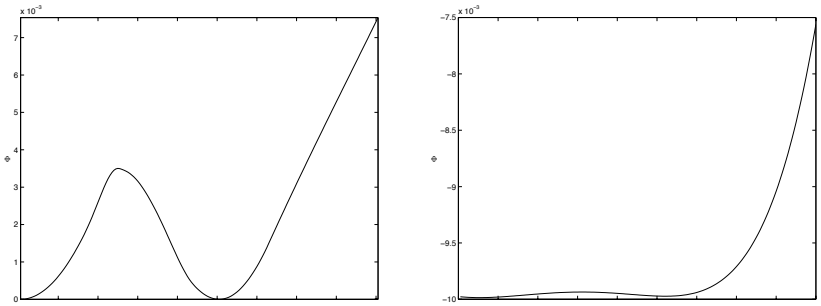

Figure 3: Section of the energy landscape. Shown is the path from the tetragonal phase (left corner) to an orthorhombic minimum. The scaling on the y-axes are both times 10^{-3}. Left: the piecewise energy defined in Section 3, with an energy barrier modeled by the biharmonic equation. Right: A lowest order polynomial ansatz determines the energy barriers via analyticity, and results in a much shallower energy barrier.

continuously differentiable box elements with element boundaries coinciding with the breaks of Table 3. These elements are three-dimensional tensor products of one-dimensional C^1 cubic Hermite-interpolation elements, thus a three-dimensional version of the Bogner-Fox-Schmitt element (Braess, 2001, Chapter II, 5.10). All degrees of freedom of the three boxes containing the minima are prescribed to ensure that the solution respects the data of Table 4. A boundary of the Finite Element domain is introduced, and the boundary conditions are set such that there is a C^1 transition to a function Φ_{large} defining Φ for large strains (see Table 4). Clearly, there is freedom in the choice of the boundary, but as soon as it is sufficiently far away from the minima, this choice will become immaterial for the simulations. We note that it would be easy to control the energy barriers between the minima as well by adding a force term to the biharmonic equation. In particular, the energy barrier is not determined via analyticity like for a polynomial ansatz of a given degree. Rather, the energy barrier can now be adjusted according to physical measurements (of *ab initio* calculations, say). To demonstrate this, compare the energy barriers for the energy defined here with those of a lowest order polynomial energy (Figure 3). The low energy barrier of the polynomial ansatz makes the correct resolution of stable phases sometimes impossible for computational investigations. See the Finite Element simulations in Section 4.

We obtain in this way a C^1 smooth energy function. Since this energy density will enter equation of motion (3) in the Finite Element simulation of Zirconia in Section 4 only in the weak formulation, we will not smoothen the energy.

We mention some fine points in the procedure described above. To deal with the nonlinear nature of the orbit space, the breaks and hence the element

Table 4: Choice of functions to fit the elastic moduli.

Tetragonal	Φ_t	=	$8.25\rho_1^2 + 161.75\rho_2 + 47.5\rho 3$
Orthorhombic	Φ_o	=	$175(\rho_1 - 0.01)^2$ $+ 7.713 \cdot 10^6(\rho_2 - 0.0001)^2 + 40\rho_3$ $- 1.6675 \cdot 10^5(\rho_1 - 0.01)(\rho_2 - 0.0001)$
Monoclinic	Φ_m	=	$222.9(\rho_1 - 0.0534)^2 + 43470(\rho_2 - 0.00232)^2$ $+ 323.7(\rho_3 - 0.0256)^2$ $- 4867(\rho_1 - 0.0534)(\rho_2 - 0.00232)$ $+ 6.942(\rho_1 - 0.0534)(\rho_3 - 0.0256)$ $- 20.27(\rho_2 - 0.00232)(\rho_3 - 0.0256)$
Large Strains	Φ_{large}	=	$150(x - 0.0267)^4 + 500(y - 0.0012)^2$ $+ 50(z - 0.0128)^2 + 0.13$

matrices are scaled according to the size of the elements on the *strain space* rather than the orbit space. This means that in direction of ρ_2 and ρ_3, where the Hilbert map is quadratic, the difference of the square roots of the coordinates is used to scale the element matrix (see Table 3). This results in an essentially equidistant scaling on the strain space. Also, it turns out to be useful to define Φ on a neighborhood of the orbit space, rather than the orbit space itself. Here, the boundaries of the domain of definition of Φ are given by $\rho_2 = 0$ and $\rho_3 = 0$. It can be shown that the definition of Φ outside the orbit space is immaterial. Indeed, all symmetry-related variants are mapped to one point in the orbit space. In particular, the corresponding parts of the boundary of a fundamental domain are identified; no further identifications on the orbit space are necessary to obtain a smooth function. This greatly facilitates the construction of an energy function.

There is arbitrariness in the definition of Φ_{large} (the values for large strains) since the physically correct growth rate is unknown. For the simulations, it is important to have a moderate growth for large strains to prevent numerical instabilities (this is one of the reasons why we have chosen not to use a polynomial energy function). The simulations will show that strains in these regions of instability disappear after a sufficiently large relaxation time.

We are mainly interested in the behavior of Zirconia at the triple point and will consequently not consider thermal effects. If one wants to do so, however, a temperature dependence could be added in the same way as for the lowest order polynomial method (Fadda et al., 2002). However, it seems advisable to pursue the piecewise approach advocated here for the dependence on temperature as well, since this might prevent the creation of additional stable phases reported by Fadda et al. (2002) for the polynomial approach.

Figures 4 and 5 show the resulting function on different planes in the strain space. We note that the energy captures the phenomenological structure of a multiphase energy with minima and energy barriers quite well.

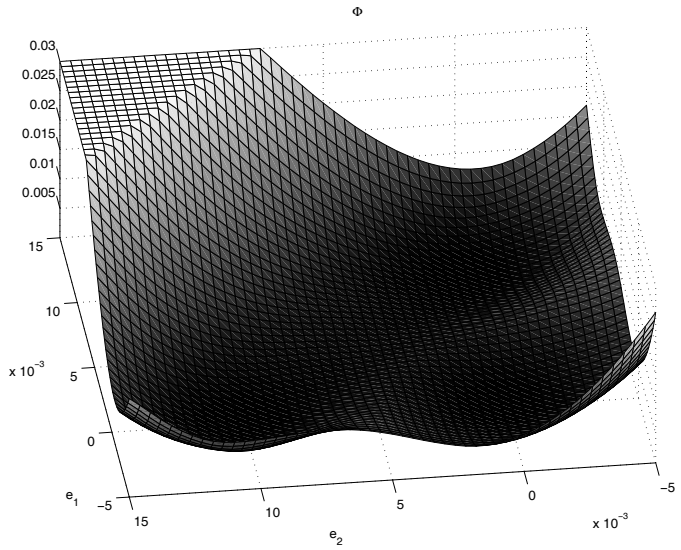

Figure 4: The tetragonal minimum in the lower right corner and the two orthorhombic minima. Shown is the plane $e_3 = 0$ in the strain space. Values larger than 0.03 have been cut for better visibility.

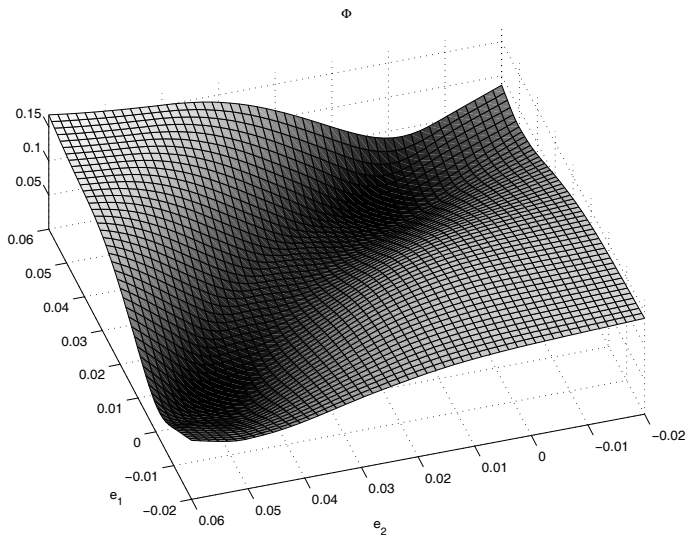

Figure 5: Two of the four monoclinic minima. Shown is the plane $e_3 = 0.16$ in the strain space.

4 Simulations

The simulations in this section will use the phenomenological energy defined in Section 3 and the methods described in that section. The pattern formation in Zirconia will be investigated and contrasted with that of a two-phase material. We first demonstrate in 4.1 that it is theoretically possible for any two of the three phases to share a phase boundary. The simulations in 4.3 will indeed exhibit all three phases in a clearly distinguishable way, as well as all combinations of neighboring phases, even with the interface penalization introduced in 4.2.

4.1 Compatibility of Phases

We first show that the three phases are mutually compatible. Two phases are compatible if there is a continuous deformation exhibiting their gradients F_1 and F_2, say, in adjacent domains. It can be shown that this is equivalent to the requirement that the matrix $D := F_2^{-T} F_1^T F_1 F_2^{-1}$ has three eigenvalues $\mu_1 \geq 1$, $\mu_2 = 1$ and $\mu_3 \leq 1$ (Bhattacharya, 2003, Chapter 5.4). Since we work in the two-dimensional framework presented in Section 2, we define *compatibility* as the reduction of the full compatibility. That is, two phases are compatible if

$$\mu_1 \geq 1, \mu_2 \leq 1, \text{ or, equivalently, } \det(D - \mathrm{Id}) \leq 0. \tag{2}$$

To show that two phases are compatible, it suffices to show that two arbitrary deformation gradients reproducing the Green-St. Venant strain tensors fulfill condition (2). The values D_{t-o}, D_{t-m} and D_{o-m}, for the tetragonal-orthorhombic, tetragonal-monoclinic and orthorhombic-monoclinic phases are easily computed from the data for $E = \frac{1}{2}(C - \mathrm{Id})$ in Table 1. It is a straightforward calculation to verify that the three phases are mutually compatible. We remark that the compatibility depends in a sensitive way on the signs involved. E.g., for a positive value of e_2 of the orthorhombic phase, the orthorhombic and the tetragonal phase are no longer compatible.

4.2 Equations of Motion and Numerical Setup

We investigate the dynamic behavior of martensitic phase transitions in Zirconia. The two-dimensional theory of phase transformations in Zirconia presented in the previous sections will be applied here. As mentioned in Section 2, the martensitic transformation under consideration can be modeled within the framework of continuum mechanics. The equations of motion are, as usual, given by the inertial Hamiltonian dynamics of the elastic deformation field $u \colon \Omega \to \mathbb{R}^2$, where $\Omega \subset \mathbb{R}^2$ is the reference configuration. In the following, x will denote the Lagrangian coordinate of a material point. The deformation gradient with respect to the material coordinate x is given by $F(x,t) := \nabla u(x,t)$. As mentioned before, we will not consider thermal effects. The non-viscous part of the Piola-Kirchhoff stress tensor is defined as

$$\sigma(F) := \frac{\partial \Phi(F)}{\partial F} \tag{3}$$

(to avoid confusion with the rotation σ defined in Section 2, we always write the argument of the stress tensor). Here, Φ will be the phenomenological energy of Section 3. The differentiation in Equation (3) is carried out in MATLAB. In particular, the energy Φ defined in Section 3 is accessible for analytic manipulations.

To resolve the non-uniqueness stemming from the non-convexity of the energy we introduce a strain-gradient term (compare Reid and Gooding (1997); Klouček and Luskin (1994)). This term serves as a penalization of the formation of interfaces; it is often coined capillarity. In a variational setting, this corresponds to an augmentation of the free energy density defined in Section 3 by a non-local Ginzburg term $\frac{\gamma}{2}|\Delta u(x,t)|^2$. This term prevents the formation of infinitely fine microstructure by introducing a length scale (Kohn and Müller, 1993). The energy minimization problem reads

$$\inf \int_\Omega \left[\alpha\Phi\left(\nabla u(x,t)\right) + \frac{\gamma}{2}|\Delta u(x,t)|^2\right] \dot{x} \tag{4}$$

with a constant $\alpha > 0$.

The corresponding (deterministic) equations of motion, augmented by an optional viscous stress $\mu\nabla u_t$, read

$$u_{tt}(x,t) = \alpha \mathrm{Div}\left(\sigma\left(\nabla u(x,t)\right)\right) - \gamma\triangle^2 u(x,t) + \mu\triangle u_t(x,t). \tag{5}$$

They will be complemented by initial values $u(x,0) = u_0$, $u_t(x,0) = v_0$ and boundary values. We write $u = (u_1, u_2)^T$ and $x = (x_1, x_2)^T$.

The term $\mu\triangle u_t(x,t)$ represents an artificial viscosity to stabilize the solution scheme. It is easy to see that this term does not represent a physical viscosity since it is not frame indifferent. However, it is widely used both in mathematical analysis (Rybka, 1992; Friesecke and Dolzmann, 1997; Zimmer, 2003b) and in numerical simulations of martensitic phase transitions. For the latter, it serves as explicit augmentation of the orientation-dependent numerical viscosity. See, e.g., Klouček and Luskin (1994) for a similar approach in two space dimensions and Swart and Holmes (1992) for a purely viscous regularization in one space dimension.

We remark that the existence of a solution of Equation (5) can be shown for moderately growing C^2 smooth energies; see Dondl (2002) for a semigroup approach.

The integration of system (5) is based on the Finite Element Method. Integration in time is carried out with an explicit scheme. Rectangular conformal Bogner-Fox-Schmitt elements are used to resolve the second order derivatives in the weak formulation of the strain-gradient term correctly. See Klouček and Luskin (1994) for a non-conforming approach for a two-phase material. It is known that non-conforming elements are suitable for the treatment of the related beam equation, and the results of Klouček and Luskin (1994) give numerical evidence that the same might hold true for Equation (5). However, at present, no proof of convergence seems to be available. We have chosen to use conforming elements since Zirconia is particularly subtle to deal with in

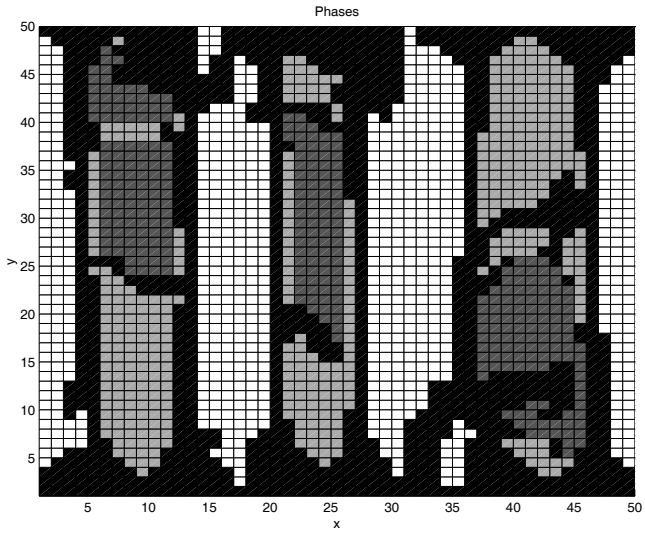

Figure 6: Relaxed state of the simulation in Section 4.3. White areas are monoclinic, light gray orthorhombic, dark gray is tetragonal. Black parts are not near an energy well.

numerical simulations. Besides having a triple point, which requires a correct resolution of all phases, the phases also have a very different scaling, with the tetragonal and the orthorhombic phases being close to each other, and the monoclinic phase being far away. The code has been implemented in MATLAB; its core is documented by Dondl (2002). We report some results.

4.3 Three Phases

The initial conditions in this experiment are chosen such that the strain is between the tetragonal and the monoclinic phase. Also, a small deviation from this state is added to prevent a relaxation in an unstable equilibrium. Figure 6 shows that the relaxed state exhibits all three phases, with oscillations between the monoclinic phase and the tetragonal and orthorhombic phases. The simulation displays the nucleation of phases starting from the perturbation in the center. The exact simulation parameters are given in Table 5. In Figure 7, the potential energy in the relaxed state is shown. Figure 8 plots the time dependence of the total, potential, kinetic, and surface energy. The orbit space variables ρ_1, ρ_2 and ρ_3 are shown in Figures 9, 10, and 11.

4.4 Orthorhombic-Tetragonal

Here we want to demonstrate once more the feasibility of the modeling approach for energies advocated in Section 3. Zirconia has been chosen as an example

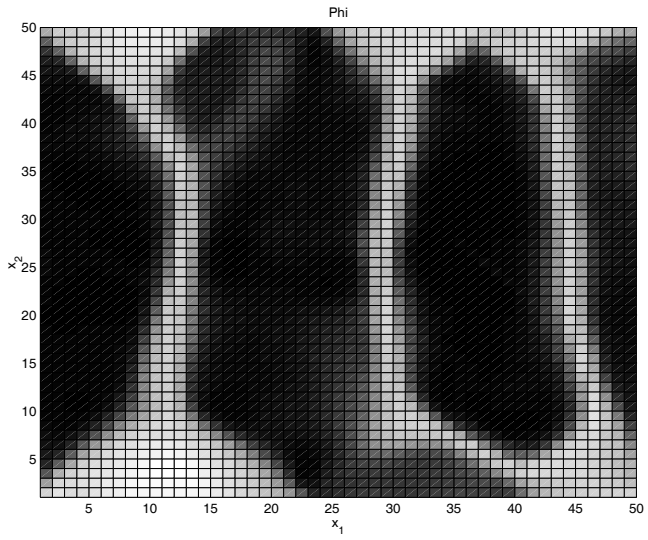

Figure 7: Potential energy in the relaxed state of the simulation in Section 4.3. One can see the higher energy (brighter) areas between the monoclinic and tetragonal/orthorhombic phases.

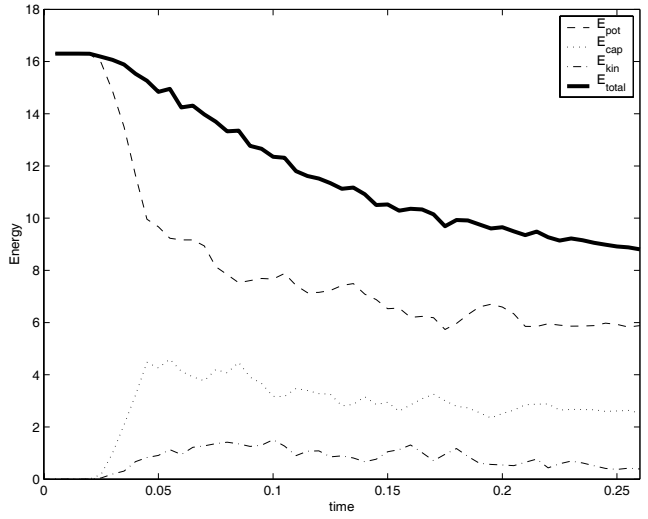

Figure 8: Evolution of total, potential, kinetic and surface (capillarity) energy with time in the simulation in Section 4.3.

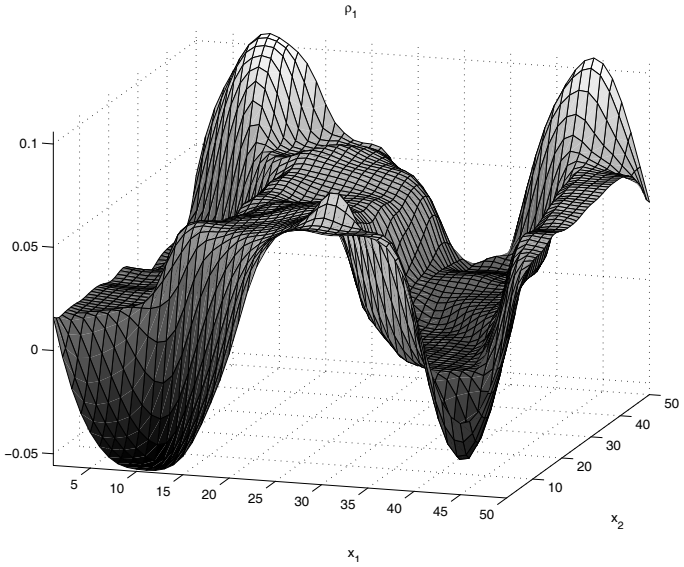

Figure 9: Relaxed state of the simulation in Section 4.3. Shown is the orbit space variable ρ_1. The intermediate strain imposed by the boundary conditions is accommodated by an oscillation between the higher strain monoclinic ($\rho_1 = 0.0534$) and the lower strain tetragonal ($\rho_1 = 0$) and orthorhombic ($\rho_1 = 0.01$) phases. Note that all three phases form plateaus.

Table 5: Simulation 4.3

Ω	$[-12.5, 12.5] \times [-12.5, 12.5]$
Grid	50×50 elements
Initial conditions	$u_1(x_1, x_2, 0) = \frac{1}{2}(0.0479x + 0.08y) + 1 \cdot 10^{-4} e^{-x^2-y^2}$
	$u_2(x_1, x_2, 0) = \frac{1}{2}(0.08x + 0.0055y) + 1 \cdot 10^{-4} e^{-x^2-y^2}$
	$u_{1,t}(x_1, x_2, 0) = u_{2,t}(x_1, x_2, 0) = 0$
Boundary conditions	Simply supported, values are initial conditions on $\partial\Omega$
α	1.0
γ	8.0
μ	0.05

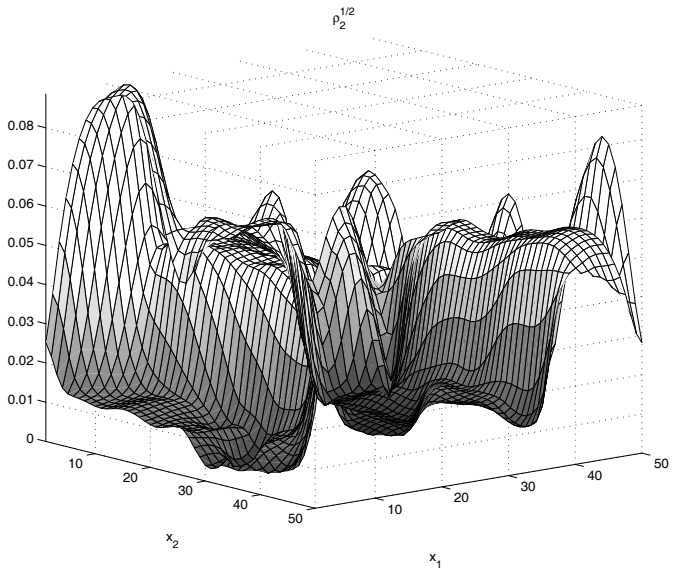

Figure 10: Relaxed state of the simulation in Section 4.3. Shown is the orbit space variable $\sqrt{\rho_2}$. The intermediate strain imposed by the boundary conditions is accommodated by an oscillation between the higher strain monoclinic ($\sqrt{\rho_2} \approx 0.0482$) and the lower strain tetragonal ($\sqrt{\rho_2} = 0$) and orthorhombic ($\sqrt{\rho_2} = 0.01$) phases. Note that all three phases form plateaus.

Table 6: The data for the simulation in Section 4.4, piecewise energy.

Ω	$[-12.5, 12.5] \times [-12.5, 12.5]$
Grid	50×50 elements
Initial conditions	$u_1(x_1, x_2, 0) = -0.01 \cdot 25 \cdot \frac{2}{\pi} \cdot \cos\left(\frac{\pi}{2} \frac{x+12.5}{25}\right)$
	$u_2(x_1, x_2, 0) = 0$
	$v_1(x_1, x_2, 0) = v_2(x_1, x_2, 0) = 0$
Boundary conditions	Simply supported, values are initial conditions on $\partial\Omega$
α	1.0
γ	8.0
μ	0.05

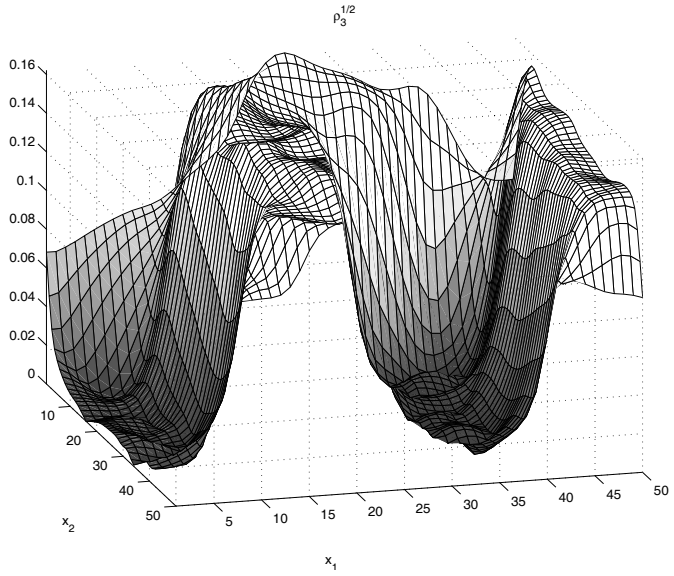

Figure 11: Relaxed state of the simulation in Section 4.3. Shown is orbit space variable $\sqrt{\rho_3}$. The values for the three minima are $\sqrt{\rho_3} = 0.16$ for the monoclinic phase and $\sqrt{\rho_3} = 0$ for the orthorhombic and the tetragonal phase.

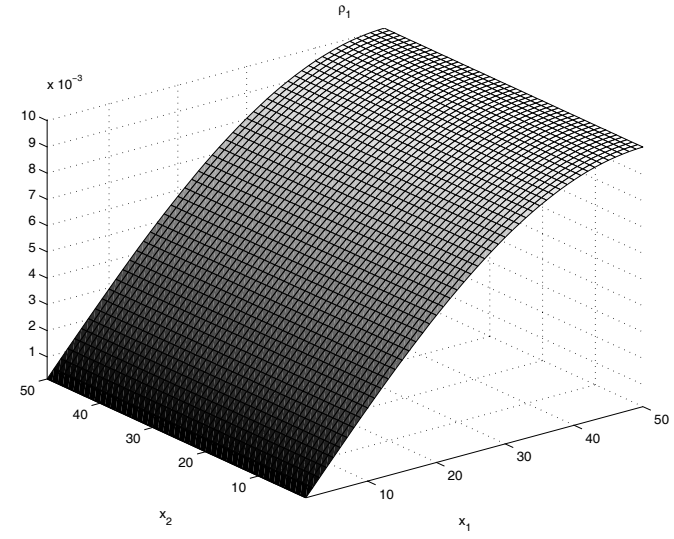

Figure 12: Initial state of the simulation in Section 4.4 with the piecewise energy function. Shown is ρ_1.

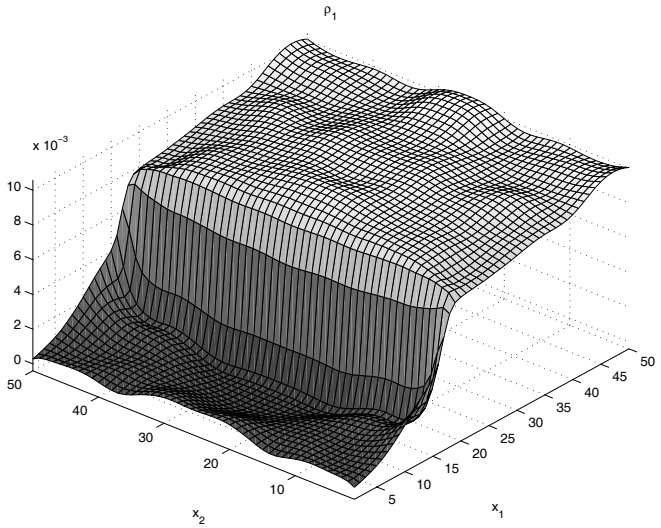

Figure 13: Relaxed state of the simulation in Section 4.4 with the piecewise energy function. Shown is ρ_1. Note the sharp phase boundary between the tetragonal ($\rho_1 = 0$) and the orthorhombic ($\rho_1 = 0.01$) phase.

since its modeling proves to be particularly subtle. The orthorhombic and the tetragonal phase are comparatively close to each other in the strain space, and even more in the orbit space (see Table 1). We want to show that the energy defined in Section 3 resolves the phenomenological structure of the landscape correctly, while a polynomial energy of lowest order does, in a numerical simulation, not yield distinguishable phases.

For the piecewise energy defined in Section 3, the initial conditions had a soft and smooth transition from strains close to the tetragonal phase for $x_1 = 0$ to strains close to the orthorhombic phase for $x_1 = 50$ (Figure 12). Figure 13 shows these intermediate strains are, for this piecewise energy, relaxed via the creation of exactly two phases. The parameters for this simulation are given in Table 6.

We contrast these simulations with the piecewise energy of Section 3 with simulations using the polynomial energy derived by Fadda et al. (2002). Precisely, we consider the restriction of their energy to the e_1, e_2, e_6-space to allow for an easy comparison of the results. Since an investigation of the energy constructed by Fadda et al. (2002) suggests that they have obtained a slightly different location of the orthorhombic phase, we modify the initial conditions slightly to ensure a fair comparison. Initial and boundary conditions are given in Table 7; the strains are close to the tetragonal phase in the lower left corner and close to the orthorhombic phase in the upper right corner. Otherwise, the data is the same as for the simulation with the piecewise energy. The results of

Table 7: The data for the simulation in Section 4.4, polynomial energy.

Ω	$[-12.5, 12.5] \times [-12.5, 12.5]$
Grid	50×50 elements
Initial conditions	$u_1(x_1, x_2, 0) = -0.0075x + 0.0085 \cdot 25 \cdot \frac{2}{\pi} \cdot \cos(\frac{\pi}{2} \frac{x+12.5}{25})$
	$u_2(x_1, x_2, 0) = -0.0075y - 0.0055 \cdot 25 \cdot \frac{2}{\pi} \cdot \cos(\frac{\pi}{2} \frac{y+12.5}{25})$
	$v_1(x_1, x_2, 0) = v_2(x_1, x_2, 0) = 0$
Boundary conditions	Simply supported, values are initial conditions on $\partial\Omega$
α	1.0
γ	8.0
μ	0.05

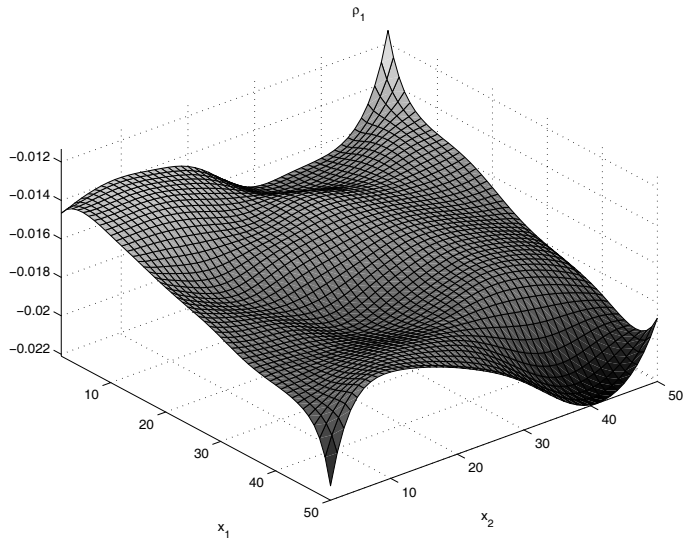

Figure 14: Relaxed state of the simulation in Section 4.4 with the polynomial energy. Shown is orbit space variable ρ_1. The simulation demonstrates that for this energy, the relaxed state does not exhibit clearly distinguishable phases. The expected values would be $\rho_1 = 0$ for the tetragonal and $\rho_1 = 0.01$ for the orthorhombic phase. Compare with the relaxed state for the piecewise function (Figure 13).

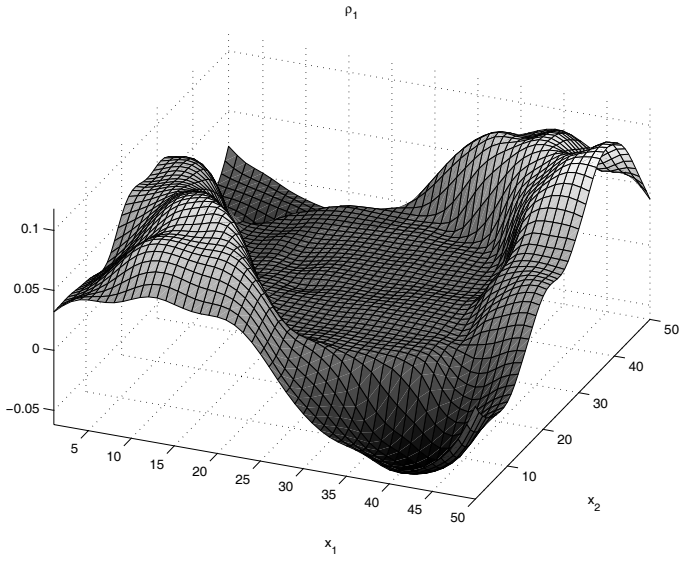

Figure 15: Relaxed state of the simulation in Section 4.5. Shown is ρ_1.

the simulation for ρ_1 are displayed in Figure 14. We notice that there are no clearly distinguishable phases. Rather, there seems to be a continuum of stable phases. This is probably a consequence of the shallow energetic landscape dictated by the polynomial approach (see Figure 3), and therefore a consequence of the insufficient height of the energy barriers. The results for the other orbit space variables ρ_2 and ρ_3 are similar to those for ρ_1, and do not yield new insights. We therefore refrain from reproducing them.

4.5 Two-phase material

We now come to the side theme mentioned in the Introduction. The previous computations are contrasted with those where the three-well energy of Section 3 is replaced by a two-well material, with wells in the tetragonal and the orthorhombic phase. The simulation will show that a three-well material like Zirconia is indeed more likely to accommodate boundary conditions by exploiting the multitude of stable phases (see Figure 6). Figure 15 shows the relaxed state for the two-phase material. Initial and boundary conditions are the same as for the three-well simulation in 4.3. See Table 5. A comparison with Figure 9 shows that the two-phase material has a large boundary layer where no local minimum is attained, while the three-phase material has few regions in locally unstable states. This can also be seen from the energy plot in Figure 16, which shows higher values than the corresponding plot for the three-phase material in Figure 8. A plot of the spatial distribution of the potential energy is given in Figure 17. It is noteworthy that the area of points with high potential energy is

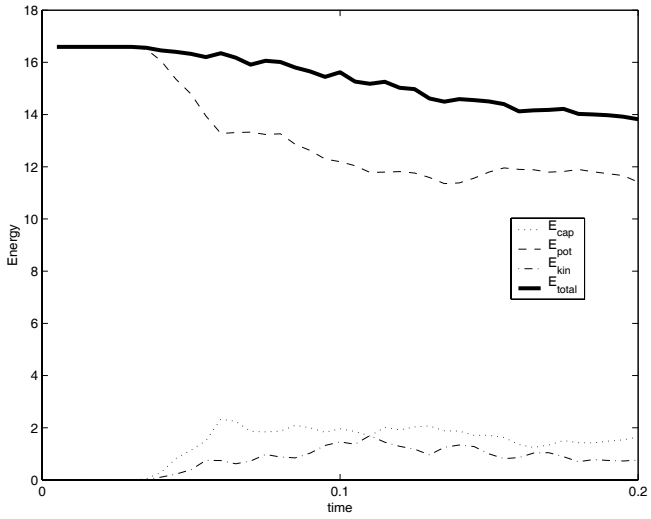

Figure 16: Evolution of total, potential, kinetic and surface (capillarity) energy with time in the simulation in Section 4.5.

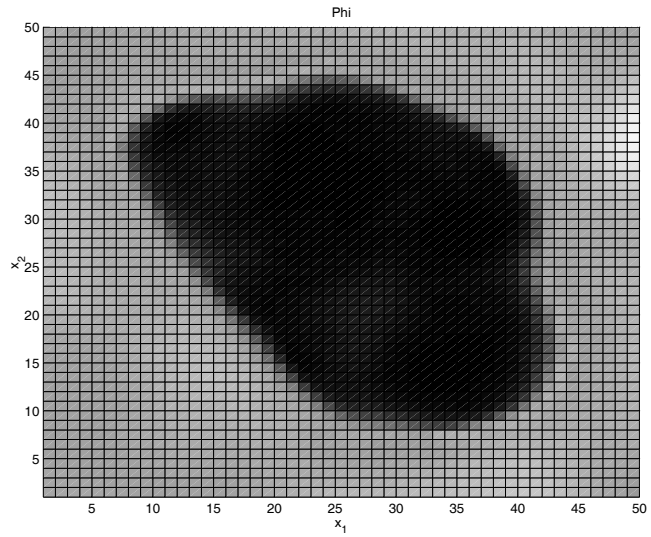

Figure 17: Potential energy Φ for the two-well energy as a function of the position. Light colors mean a high potential energy. This figure is to be contrasted with Figure 7. There, the three wells allow for a much better accommodation of the boundary conditions, having essentially only phase boundaries as regions with high potential energy.

significantly larger than for the corresponding three-well simulation (Figure 7). These results suggest that the set of recoverable strains of a three-phase material can be significantly larger that that of a material with two of the three wells.

5 Discussion

The energy derived in Section 3 meets the symmetry requirements of the tetragonal-orthorhombic-monoclinic phase transition in Zirconia, and it interpolates experimental data that is available for this material in the two-dimensional frameworks of Section 2. The Finite Element simulations in Section 4 show, among others, the feasibility of this approach by exhibiting all three phases in a clearly distinguishable manner.

One of our goal here is to present the orbit space method combined with a piecewise approach as an alternative to the global polynomial ansatz commonly used in Landau theory. In Section 1, it is explained that invariant polynomials are very well suited for the local energetic description they were originally intended for, but not do not necessarily describe the global picture of the energy landscape appropriately. The approach presented here provides a natural extension of the local polynomial picture to a global one. Besides being simple, it also comprises the results obtainable with a purely polynomial approach. The Hilbert basis for a given symmetry can be computed automatically; the function Φ of this symmetry base is defined in a local way by evaluating all available local data and interpolating appropriately.

The idea to derive energy functions by using a Finite Element simulation seems to be new. In geometric modeling, this method has been used successfully to construct surfaces without unwanted minimizers (by solving Laplace's equation), or surfaces with minimal curvature (by solving the biharmonic equation). See, e.g., Bloor and Wilson (1991) for the use of partial differential equations in geometric modeling.

The approach presented here allows the derivation of elastic energies that faithfully reproduce the symmetry of the phases, the position of the phases and their elastic moduli. This opens the way of studying the relaxation of these energies in a systematic way. In particular, the orbit space might turn out to be a useful tool. A success might eventually lead to the prediction of the constitutive response for smart materials.

We stress that the methods of deriving energy functions presented here are more general in scope, and offer the potential of fitting large numbers of parameters, such as atomistic potentials for molecular dynamics.

Acknowledgments

The results presented here grew out of a part of PWD's Master's thesis in theoretical physics at the Technische Universität München, Germany. The work

was carried out while JZ was a postdoctoral scholar at the California Institute of Technology and PWD was a special student at the same institution. He thanks Kaushik Bhattacharya for support, and the Division of Engineering and Applied Sciences at Caltech for hospitality. We gratefully acknowledge the financial support of the US Air Force Office of Scientific Research through a MURI grant (F49620-98-1-0433) and an NSF-ITR grant (ACI-0204932).

Both authors thank Kaushik Bhattacharya for helpful discussions, encouragement, and generous support. We are also grateful for stimulating discussions with Lev Truskinovsky and Giovanni Zanzotto; they kindly provided drafts (Truskinovsky and Zanzotto, 2002; Fadda et al., 2002), from which we greatly benefited.

References

Balk, A. M., Cherkaev, A. V., Slepyan, L. I., 2001. Dynamics of chains with non-monotone stress-strain relations. I. Model and numerical experiments. J. Mech. Phys. Solids 49 (1), 131–148.

Bhattacharya, K., 2003. Martensitic Phase Transformations. Oxford University Press.

Bloor, M. I. G., Wilson, M. J., 1991. Partial differential equations for shape generation in geometric modelling. In: Geometry and topology of submanifolds, III (Leeds, 1990). World Sci. Publishing, River Edge, NJ, pp. 32–48.

Braess, D., 2001. Finite elements, 2nd Edition. Cambridge University Press, Cambridge, theory, fast solvers, and applications in solid mechanics, Translated from the 1992 German edition by Larry L. Schumaker.

Chevalley, C., 1955. Invariants of finite groups generated by reflections. Amer. J. Math. 77, 778–782.

Dondl, P., 2002. Modeling and analysis of non-diffusive structural phase transitions in solids. Master's thesis, Technische Universität München.

Ericksen, J. L., 1980. Some phase transitions in crystals. Arch. Rational Mech. Anal. 73 (2), 99–124.

Fabris, S., Paxton, A. T., Finnis, M. W., 2000. Relative energetics and structural properties of zirconia using a self-consistent tight-binding model. Phys. Rev. B 61 (10), 6617–6630.

Fadda, G., Truskinovsky, L., Zanzotto, G., 2002. Unified Landau description of the tetragonal, orthorhombic, and monoclinic phases of zirconia, submitted.

Friesecke, G., Dolzmann, G., 1997. Implicit time discretization and global existence for a quasi-linear evolution equation with nonconvex energy. SIAM J. Math. Anal. 28 (2), 363–380.

Gooding, R. J., Ye, Y. Y., Chan, C. T., Ho, K. M., Harmon, B. N., 1991. Role of non-symmetry-breaking order parameters in determining the martensitic energy barrier: The bcc-to-9R transformation. Phys. Rev. B 43 (16), 13 626–13 629.

Greuel, G.-M., Pfister, G., Schönemann, H., 2001. SINGULAR 2.0. A Computer Algebra System for Polynomial Computations, Centre for Computer Algebra, University of Kaiserslautern, `http://www.singular.uni-kl.de`.

Gurtin, M. E. (Ed.), 1984. The Cauchy and Born hypotheses for crystals. Academic Press Inc., Orlando, FL.

Huo, Y., Müller, I., 2003. Interfacial and inhomogeneity penalties in phase transitions, to appear in *Contin. Mech. Thermodyn.*

Klouček, P., Luskin, M., 1994. Computational modeling of the martensitic transformation with surface energy. Math. Comput. Modelling 20 (10-11), 101–121.

Kohn, R. V., Müller, S., 1993. Surface energy and the length scale of twinning in martensite. In: Wayman, C. M., Perkins, J. (Eds.), Proceedings of the International Conference on Martensitic Transformations (1992). Monterey Institute of Advanced Studies, Carmel, California, pp. 77–81.

Landau, L. D., 1967. On the theory of phase transitions. In: Haar, D. T. (Ed.), Collected papers of L. D. Landau. Gordon and Breach Science Publishers, New York.

Luskin, M., 1996. On the computation of crystalline microstructure. In: Acta numerica, 1996. Cambridge Univ. Press, Cambridge, pp. 191–257.

Ondik, H. M., McMurdie, H. F. (Eds.), 1998. Phase Diagrams for Zirconium and Zirconia Systems. American Ceramic Society, Westerville, OH.

Pitteri, M., 1984. Reconciliation of local and global symmetries of crystals. J. Elasticity 14 (2), 175–190.

Reid, A., Gooding, R., 1997. Pattern formation in a 2D elastic solid. Physica A 239 (1-3), 1–10.

Rybka, P., 1992. Dynamical modelling of phase transitions by means of viscoelasticity in many dimensions. Proc. Roy. Soc. Edinburgh Sect. A 121 (1-2), 101–138.

Smith, G. F., Rivlin, R. S., 1958. The strain-energy function for anisotropic elastic materials. Trans. Amer. Math. Soc. 88, 175–193.

Sturmfels, B., 1993. Algorithms in invariant theory. Springer-Verlag, Vienna.

Swart, P. J., Holmes, P. J., 1992. Energy minimization and the formation of microstructure in dynamic anti-plane shear. Arch. Rational Mech. Anal. 121 (1), 37–85.

Truskinovsky, L., Zanzotto, G., 2002. Elastic crystals with a triple point. J. Mech. Phys. Solids 50 (2), 189–215.

Weyl, H., 1997. The classical groups. Princeton University Press, Princeton, NJ, their invariants and representations, Fifteenth printing, Princeton Paperbacks.

Zimmer, J., 2003a. Stored energy functions for phase transitions in crystals, accepted for publication in *Archive for Rational Mechanics and Analysis*.

Zimmer, J., 2003b. Thermo-viscoelasticity with nonconvex energy, submitted to *Journal of Mathematical Analysis and Applications*.